A Universal DNA Aptamer as an Efficient Inhibitor against Spike Protein/hACE2 interactions

SCHOLARONE™
Manuscripts

COMMUNICATION

A Universal DNA Aptamer as an Efficient Inhibitor against Spike-Protein/hACE2 interactions

Achut Prasad Silwal, Raunak Jahan, Siddhartha Kalpa Samadhi Thennakoon, Satya Prakash Arya, Rick Mason Postema, Elizabeth Claire VanderArk, and Xiaohong Tan*

A universal aptamer against spike-proteins of diverse SARS-CoV-2 variants was discovered via DNA SELEX towards the wild-type (WT) spike-protein. This aptamer, A1C1, binds to the WT spike-protein or other variants of concern such as Delta and Omicron with low nanomolar affinities. A1C1 inhibited the interaction between hACE2 and various spike-proteins by 85-89%. This universal A1C1 aptamer can be used to design diagnostic and therapeutic molecular tools to target SARS-CoV-2 and its variants.

Severe acute respiratory syndrome coronavirus 2 (SARS-CoV-2) uses its spike-protein to attach to the host cell via human angiotensin converting enzyme 2 (hACE2). The viral infection can be stopped by designing an inhibitor that can block the interaction between the spike-protein and hACE2. As shown in Figure 1, one spike-protein trimer includes three spike-proteins, and each of them is composed of the subunits S1 and S2. S1 consists of S1A and S1B (Figure 1A), in which S1B, also called the receptor-binding domain (RBD), establishes the direct interaction with hACE2.[1] Additionally, the S2 subunit plays a function in mediating the fusion of the viral membrane to the host cell. Therefore, virus entry is accomplished via a cascade of events, *i.e.*, S1 binds to hACE2, which then triggers S2 to change its conformation to a more stable post-fusion state and allows viral entry into the host cell.[2–4] Since S1 directly interacts with hACE2, many research groups have been actively working to discover various biomolecules such as antibodies[5–10] or aptamers[11–16] to effectively block the interaction between S1 and hACE2.

Aptamers are single-stranded oligonucleotides that can fold into complex 3D structures, enabling them to specifically recognize unique targets, including proteins, nucleic acids, small molecules, and even cells.[17–19] Aptamers are selected from a large random pool of polynucleotides via an iterative selection process called Systematic Evolution of Ligands by Exponential Enrichment (SELEX).[20,21] DNA aptamers are less expensive to produce than antibodies and can be manufactured using general chemical

Department of Chemistry and Center for Photochemical Sciences, Bowling Green State University, Bowling Green, Ohio 43403, United States
† To whom correspondence should be addressed: tanx@bgsu.edu
Electronic Supplementary Information (ESI) available: [Experimental methods and supporting Figures and Tables]. See DOI: 10.1039/x0xx00000x
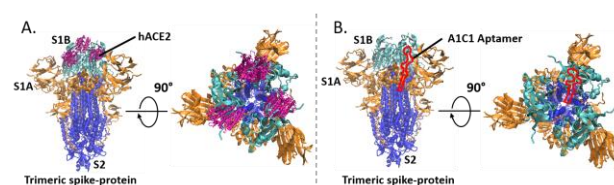
Figure 1. The schematic representation of the interplay between the wild type SARS-CoV-2 spike-protein, hACE2 and A1C1 aptamer (not in a scale). (A) The interaction between the trimeric spike-protein and hACE2. The three S1B, S1A, and S2-subunits of the trimeric spike-protein are depicted in cyan, orange, and blue colors, respectively (PDB code 6vxx). The hACE2 (PBD code 6mOj) is depicted in magenta color. (B) Demonstration of SARS-CoV-2 neutralization using the A1C1 aptamer (red). The actual binding site of A1C1 on spike-protein is uncertain.

synthesis.[22–27] DNA aptamers also have low immunogenicity, in comparison to antibodies; hence, DNA aptamers can be a useful molecular tool in disease therapeutics and diagnostics.

In this work, we used the WT spike-protein as the target and performed an *in vitro* selection to isolate aptamers (Figure 2A). The initial pool of DNA libraries contained ~10^{15} unique sequences of a 40-nucleotide randomized region. After each round of selection, the winner DNA library was amplified by PCR reaction. After the second selection round, the counter-selection with the unembellished Ni-NTA magnetic beads was employed to remove the nonspecific library in every other selection round. The additional details of the selection process are provided in Figure S1 and Table S1. Moreover, we incrementally decreased the target to library ratio from 2.4: 1 in round 1 to 1: 5 in round 10 to favor the selection of high-affinity anti-spike-protein aptamers. After 10 rounds of *in vitro* selection, the enriched library was obtained (Figure S1). The binding capabilities of all enriched DNA toward spike-protein were evaluated by a fluorescence plate reader after the 7th selection round. Briefly, the 6-FAM-ssDNA was subjected to bind to the His-tagged WT spike-protein coupled with anti-His-tagged biotinylated sera-mag magnetic streptavidin-coated beads (Figure S2A). After washing, the 6-FAM-ssDNA library was eluted from the complex, and fluorescence
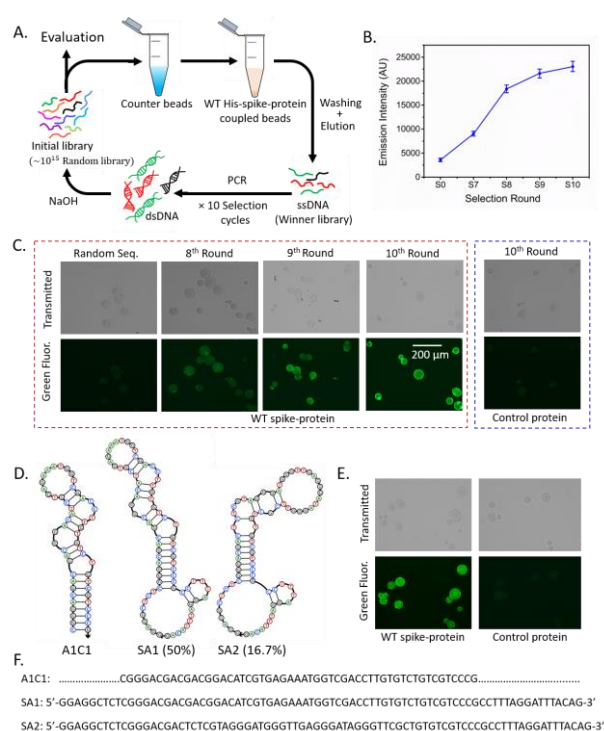
Figure 2. Selection and characterization of anti-spike DNA aptamers. (A) SELEX scheme for the selection of aptamers against the WT spike-protein. (B) The fluorescence intensity of the ssDNA library increased over selection rounds, indicating the enhanced binding capability. The fluorescence emission was measured at λ_{max} = 520 nm. (C) Fluorescence imaging of spike-protein/Ni-NTA beads in the presence of the 6-FAM-ssDNA library. The libraries were obtained from the 0th, 7th, 8th, 9th, and 10th rounds, respectively. It shows that the spike-specific pool is satisfactorily enriched after the 10th round of selection. The control protein does not display a fluorescence signal. (D) The secondary structures of the anti-spike aptamers were obtained using NUPACK. (E) Fluorescence image of the 6-FAM-A1C1 aptamer and Ni-NTA resin beads coupled with the WT spike-protein and control protein. Brighter fluorescence images from the beads coupled with the WT spike-protein shows that the 6-FAM-A1C1 specifically and effectively bound to the WT spike-protein. (F) Nucleotide sequences of the anti-spike aptamers. The A1C1 aptamer was optimized from SA1 by deleting redundant nucleotides (dotted ones) while aptamers SA1 and SA2 are the original aptamers obtained via selection process.

emission (λ_{max} = 520 nm) was measured using the Clariostar microplate reader. As shown in Figure 2B, the fluorescence signal significantly increased from the 7th round to the 8th round, and it consistently increased to its maximum at the 10th round. In addition, the His-tagged spike-protein was immobilized on a nickel-nitrilotriacetic acid (Ni-NTA) resin and incubated with 6-FAM-ssDNAs (Figure S2B). After washing, the resin was subjected to fluorescence imaging. As shown in Figure 2C and Table S2, the pool from the 9th and 10th rounds displayed a stronger fluorescent signal in comparison to the 8th round. Furthermore, the 6-FAM-labeled ssDNA from the 10th round did not bind to the control His-tagged protein immobilized on the Ni-NTA resin. This implies that there is high

binding capability and specificity of the ssDNA library from the 10th round toward the spike-protein. The above data indicate that after 10 rounds of SELEX, we obtained a promising aptamer candidate pool with good binding ability against the spike-protein. For this reason, the enriched aptamer candidate pool from the 10th round was cloned using a TOPO TA Cloning® Kit. The product of recombination was used to transform *E. coli* component cells, and random colonies were sequenced (Figure S3). The 50 % and 16.7 % of the total sequence data were occupied by SA1 and SA2 sequences, respectively (Table S3). Both consensus sequence motifs contained multiple GGG, GG, CCC, or CC repeats. The secondary structures of all aptamers are shown in Figure 2D. In addition, we also determined the specific binding of the 6-FAM-labeled A1C1 on spike-protein using fluorescence microscopy (Figure 2E). For fluorescence imaging, the Ni-NTA/WT spike-protein complex was incubated with 100 nM 6-FAM-A1C1 DNA for 30 minutes and washed 3 times before collecting fluorescence images by a digital inverted fluorescence microscope (Invitrogen EVOS FL). The bright fluorescence image was observed from the Ni-NTA/WT spike-protein complex in the presence of the 6-FAM-A1C1 aptamer or the 6-FAM-ssDNA obtained from the 10th round of selection. However, both failed to provide the noticeable bright image when WT spike-protein was replaced by control protein keeping all other experimental conditions the same. These experimental results indicate that A1C1 is specifically bound against WT spike-protein with potentially high affinity. We optimized the predominant sequence SA1, originally obtained by the selection process, by deletion of redundant nucleotides to obtain the aptamer A1C1. The sequences of all aforementioned aptamers are provided in Figure 2F.

Next, the binding capability of the A1C1 aptamer toward the WT spike-protein was further evaluated by the gold nanoparticle (AuNPs) based colorimetric assay (Figure S4A). The detailed mechanism and kinetics of the interaction between aptamer and AuNPs that prevents AuNPs from aggregating have been extensively characterized by Nelson and Rothberg.[28] In this work, briefly, when the WT spike-protein was added into the colloids of AuNPs, NaCl, and A1C1 aptamers, the A1C1 aptamer was preferably bound to WT spike-protein causing the aggregation of AuNPs. The wine-red color of the AuNPs colloids was intact for more than 48 hours in the presence of 1.5 M NaCl and 250 nM A1C1 aptamer. However, it dramatically changed into blue or purple color within 5 minutes of adding 250 nM of the WT spike-protein (Figure S4B). Besides visual color change, UV-Vis measurement was also employed to measure the effect of various proteins to the colloids of AuNPs, A1C1, and NaCl (Figure S4C). The WT spike-protein caused the significant redshift of the characteristic peak of AuNPs colloids located at 520 nm. The WT S1 and WT S2-proteins also caused some redshift to the 520 nm peak, but it was not as obvious as the redshift caused by the WT spike-protein. This states that A1C1 preferably binds to the intact WT spike-protein over the single WT S1 or S2 protein. Next, we performed the fluorescence imaging study on Ni-NTA resin beads coupled with the His-
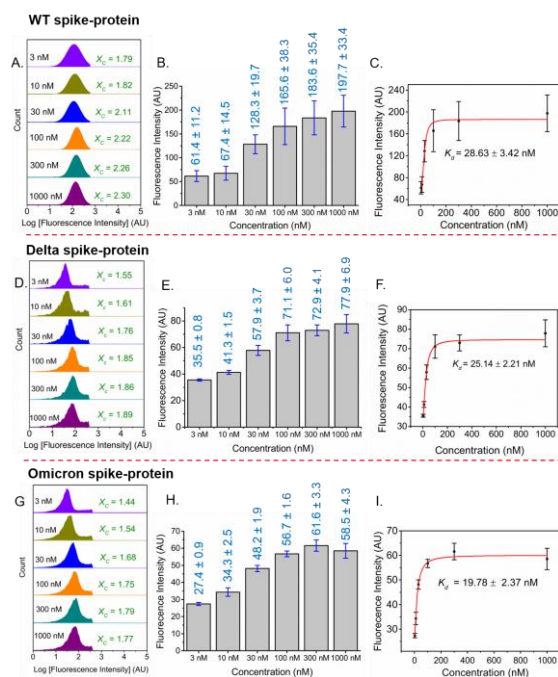
Figure 3. The binding affinity of the 6-FAM-A1C1 aptamer against the (A-C) WT, (D-F) Delta, and (G-I) Omicron spike-protein. (A, D, and G) The mean green fluorescence emission intensity (X_C) measured by the flow cytometry from the 6-FAM-A1C1 aptamer bound to the complex of Ni-NTA bead and His-tagged spike-protein. (B, E, and H) The increment of X_C values as a function of 6-FAM-A1C1 concentration bound to the virtually same quantity of Ni-NTA bead/spike-protein complex. The error bars indicate the standard deviation of X_C values from the mean X_C value of three trials (C, F, and I) The binding affinity (K_d) of the 6-FAM-A1C1 aptamer against spike-protein was determined by intensity vs concentration plot using the Origin software.

tagged S1, S2, WT spike-protein, and a control protein (PD-L1), in the presence of the 6-FAM-A1C1 aptamer. Figure S5 shows that the A1C1 aptamer has no binding to the control protein. It shows weaker but comparable binding to isolated S1 or S2, and much stronger binding to the intact spike-protein. The quantification analysis indicates that, binding to the 6-FAM-A1C1 aptamer, S1, S2, PD-L1, and unembellished Ni-NTA resin bead shows 34.4, 31.9, 7.6, and 5.5 % fluorescence intensity, respectively, in comparison to the normalized 100 % fluorescence intensity produced by the intact WT spike-protein (Figure S5C). Since A1C1 still can bind to S1 or S2 alone, we assume that A1C1 may bind to the junction site of S1 and S2 in the whole spike-protein. Further study on the complex structure can provide more information.

To test the binding affinity of the A1C1 against WT, Delta, and Omicron spike-proteins, we employed the flow cytometry assay using the Ni-NTA magnetic beads (Figure 3). The beads were incubated with 200 nM target protein for 2 h, and it was washed with the SELEX buffer. The Ni-NTA/protein complex was then incubated with various concentrations (3, 10, 30, 100, 300, and
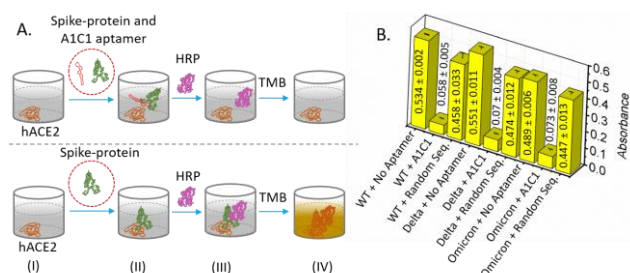
Figure 4. The determination of the inhibition efficacy of the A1C1 aptamer against the hACE2/spike-proteins interaction. (A) The schematic representation of the ELISA competition assay to measure the inhibition efficacy of the aptamers (not to the scale). The hACE2 is first coated to the well surface (I); when the mixture of A1C1 aptamer and His-tagged spike-protein (top panel) is added to the well, the binding potential of hACE2/spike-protein interaction competes with the A1C1/spike-protein interaction (II); since potential of the A1C1/spike-protein interactions exceeds that of hACE2/spike-protein interaction, the spike-protein and HRP do not persist in the well after washing (III); in the absence of HRP, TMB does not produces any color product (top panel). However, in the absence of aptamer hACE2 has strong interaction with spike-protein, and color product is formed (bottom panel). (B) The inhibition efficacy of the A1C1 aptamer or random DNA sequence is determined as an opposite function of the absorbance caused by the color product. The blue color is formed due to TMB mediated oxidation of HRP, which changes into yellow after adding 2 μL of concentrated sulfuric acid. The absorbance is measured by employing Clariostar microplate reader at λ_{max} = 450 nm. For each sample, ELISA test was performed for three trials. The error bars indicate the standard deviation of the absorbance from their mean observed in three trials. The A1C1 aptamer inhibits approximately 89.1, 87.3, and 85 % of hACE2/spike-protein interactions related to the WT, Delta, and Omicron respectively.

1000 nM) of the 6-FAM-A1C1 aptamer, and samples were subjected to the flow cytometry measurement after washing. When the A1C1 concentration was 3 nM, the Ni-NTA bead/protein complex produced a weaker fluorescence signal. As A1C1 concentration was increased from 3 to 100 nM range, the fluorescence signal was significantly increased. However, it did not apparently change when A1C1 concentration was increased beyond the range of 100 nM. As shown in Figure 3, A1C1 has a low nanomolar binding affinity toward different spike-proteins. The K_d values of A1C1 aptamers are 28.6, 25.1, and 19.8 nM, for the WT, Delta, and Omicron spike-proteins, respectively.

Finally, The A1C1 aptamer was tested for its ability to block the hACE2/spike-protein interaction in an ELISA competition assay (Figure 4A). Briefly, the ELISA wells were first coated with the hACE2 protein. The A1C1 aptamer and spike-proteins (WT, Delta, or Omicron) were then added simultaneously to the well to measure the competition of the hACE2/spike-protein binding

over the A1C1/spike-protein interaction. After washing, the amount of the residual spike-protein in each well was determined using the absorbance caused by the HRP-mediated oxidation of the TMB. The amount of anti-His-tagged-HRP apparently relies on the residual spike-protein that bind to hACE2. Additional control experiments were performed in the absence of the A1C1 aptamer or using a control pool of the random ssDNA library obtained from the 1st round selection. The analysis from the ELISA competition assay showed that approximately 89.1 % of WT, 87.3 % of Delta, and 85 % of Omicron spike-protein interactions with hACE2 were inhibited by the A1C1 aptamer, respectively (Table S4, Figures 4B and S6). The control experiments confirm that the hACE2/spike-protein interaction can only be specifically inhibited by A1C1. Recently, it was reported that the SP6 aptamer does not bind to the RBD of the S1-protein, but it reduces pseudovirus infection by interfering with the post-binding process of the pseudovirus to cells via an RBD-independent mechanism.[29] The inhibition mechanism of our A1C1 is currently unknown. Most likely once A1C1 binds to the spike-protein, it induces an allosteric effect on spike-protein, affecting its binding with hACE2.

In summary, we isolated anti-spike-protein aptamers by *in vitro* selection. The selected universal anti-spike protein aptamer, A1C1, binds to WT, Delta, and Omicron spike-protein with uniformly high affinity. Furthermore, the A1C1 aptamer can inhibit 85-89.1% of the hACE2/spike-protein interaction including WT, Delta, and Omicron variants. Conclusively, the anti-spike-protein universal A1C1 aptamer could be used to design diagnostic and therapeutic molecular tools to target SARS-CoV-2 and its variants.

Acknowledgement

X.T., and A.S. designed research; A.S., R.J., S.T., S.A., R.M., E.V., and X.T. performed research and analyzed data; and X.T., and A.S. wrote the paper with contributions from all authors.

There are no conflicts of interest to declare.

References

1   C. O. Barnes, A. P. West Jr, K. E. Huey-Tubman, M. A. G. Hoffmann, N. G. Sharaf, P. R. Hoffman, N. Koranda, H. B. Gristick, C. Gaebler and F. Muecksch, *Cell*, 2020, **182**, 828-842. e16.
2   M. Gui, W. Song, H. Zhou, J. Xu, S. Chen, Y. Xiang and X. Wang, *Cell Res.*, 2017, **27**, 119–129.
3   W. Song, M. Gui, X. Wang and Y. Xiang, *PLoS Pathog.*, 2018, **14**, e1007236.
4   R. N. Kirchdoerfer, N. Wang, J. Pallesen, D. Wrapp, H. L. Turner, C. A. Cottrell, K. S. Corbett, B. S. Graham, J. S. McLellan and A. B. Ward, *Sci. Rep.*, 2018, **8**, 1–11.
5   C. Wang, W. Li, D. Drabek, N. Okba, R. van Haperen, A. D. M. E. Osterhaus, F. J. M. van Kuppeveld, B. L. Haagmans, F. Grosveld and B.-J. Bosch, *Nat. Commun.*, 2020, **11**, 1–6.
6   B. Ju, Q. Zhang, J. Ge, R. Wang, J. Sun, X. Ge, J. Yu, S. Shan, B. Zhou and S. Song, *Nature*, 2020, **584**, 115–119.
7   R. Shi, C. Shan, X. Duan, Z. Chen, P. Liu, J. Song, T. Song, X. Bi, C. Han and L. Wu, *Nature*, 2020, **584**, 120–124.
8   L. Liu, P. Wang, M. S. Nair, J. Yu, M. Rapp, Q. Wang, Y. Luo, J. F.-W. Chan, V. Sahi and A. Figueroa, *Nature*, 2020, **584**, 450–456.
9   J. Huo, A. Le Bas, R. R. Ruza, H. M. E. Duyvesteyn, H. Mikolajek, T. Malinauskas, T. K. Tan, P. Rijal, M. Dumoux and P. N. Ward, *Nat. Struct. Mol. Biol.*, 2020, **27**, 846–854.
10   M. Schoof, B. Faust, R. A. Saunders, S. Sangwan, V. Rezelj, N. Hoppe, M. Boone, C. B. Billesbølle, C. Puchades and C. M. Azumaya, *Science (80-.).*, 2020, **370**, 1473–1479.
11   X. Liu, Y. Wang, J. Wu, J. Qi, Z. Zeng, Q. Wan, Z. Chen, P. Manandhar, V. S. Cavener and N. R. Boyle, *Angew. Chemie Int. Ed.*, 2021, **60**, 10273–10278.
12   G. Yang, Z. Li, I. Mohammed, L. Zhao, W. Wei, H. Xiao, W. Guo, Y. Zhao, F. Qu and Y. Huang, *Signal Transduct. Target. Ther.*, 2021, **6**, 1–4.
13   M. Sun, S. Liu, X. Wei, S. Wan, M. Huang, T. Song, Y. Lu, X. Weng, Z. Lin and H. Chen, *Angew. Chemie*, 2021, **133**, 10354–10360.
14   J. Valero, L. Civit, D. M. Dupont, D. Selnihhin, L. S. Reinert, M. Idorn, B. A. Israels, A. M. Bednarz, C. Bus and B. Asbach, *Proc. Natl. Acad. Sci.*, , DOI:https://doi.org/10.1073/pnas.2112942118.
15   M. Sun, S. Liu, T. Song, F. Chen, J. Zhang, J. Huang, S. Wan, Y. Lu, H. Chen and W. Tan, *J. Am. Chem. Soc.*, 2021, **143**, 21541–21548.
16   Z. Zhang, J. Li, J. Gu, R. Amini, H. D. Stacey, J. C. Ang, D. White, C. D. M. Filipe, K. Mossman, M. S. Miller, B. J. Salena, D. Yamamura, P. Sen, L. Soleymani, J. D. Brennan and Y. Li, *Chem. – A Eur. J.*, 2022, **28**, e202200524.
17   J. J. F. Verhoef, J. F. Carpenter, T. J. Anchordoquy and H. Schellekens, *Drug Discov. Today*, 2014, **19**, 1945–1952.
18   K. W. Thiel and P. H. Giangrande, *Oligonucleotides*, 2009, **19**, 209–222.
19   P. R. Bouchard, R. M. Hutabarat and K. M. Thompson, *Annu. Rev. Pharmacol. Toxicol.*, 2010, **50**, 237–257.
20   C. Tuerk and L. Gold, *Science (80-.).*, 1990, **249**, 505–510.
21   A. D. Ellington and J. W. Szostak, *Nature*, 1990, **346**, 818–822.
22   M. McKeague, E. M. McConnell, J. Cruz-Toledo, E. D. Bernard, A. Pach, E. Mastronardi, X. Zhang, M. Beking, T. Francis and A. Giamberardino, *J. Mol. Evol.*, 2015, **81**, 150–161.
23   A. Ruscito and M. C. DeRosa, *Front. Chem.*, 2016, **4**, 14.
24   S. J. Klug and M. Famulok, *Mol. Biol. Rep.*, 1994, **20**, 97–107.
25   R. Stoltenburg, C. Reinemann and B. Strehlitz, *Biomol. Eng.*, 2007, **24**, 381–403.
26   M. F. Polz and C. M. Cavanaugh, *Appl. Environ. Microbiol.*, 1998, **64**, 3724–3730.
27   M. Takahashi, X. Wu, M. Ho, P. Chomchan, J. J. Rossi, J. C. Burnett and J. Zhou, *Sci. Rep.*, 2016, **6**, 1–14.
28   E. M. Nelson and L. J. Rothberg, *Langmuir*, 2011, **27**, 1770–1777.
29   A. Schmitz, A. Weber, M. Bayin, S. Breuers, V. Fieberg, M. Famulok and G. Mayer, *Angew. Chemie Int. Ed.*, 2021, **60**, 10279–10285.